PREPRINT 507

OCTOBER 2020

igpm | RWTH AACHEN UNIVERSITY

Well-balanced discontinuous Galerkin scheme for 2 × 2 hyperbolic balance law

Yogiraj Mantri* and Sebastian Noelle§

Institut für Geometrie und Praktische Mathematik
Templergraben 55, 52062 Aachen, Germany

* Institut für Geometrie und Praktische Mathematik, RWTH Aachen University, Aachen, Germany (mantri@eddy.rwth-aachen.de).
§ Institut für Geometrie und Praktische Mathematik, RWTH Aachen University, Aachen, Germany (noelle@igpm.rwth-aachen.de).

Well-balanced discontinuous Galerkin scheme for 2×2 hyperbolic balance law

Yogiraj Mantri* and Sebastian Noelle

Institut für Geometrie und Praktische Mathematik,
RWTH Aachen University,
Templergraben 55, 52056 Aachen, Germany.

Abstract

The numerical solutions to nonlinear hyperbolic balance laws at (or near) steady state may develop spurious oscillations due to the imbalance between flux and source terms. In the present article, we study a high order well-balanced discontinuous Galerkin (DG) scheme for balance law with subsonic flow, which preserves equilibrium solutions of the flow exactly, and also provides non-oscillatory solutions for flow near equilibrium. The key technique is to reformulate the DG scheme in terms of global equilibrium variables which remain constant in space and time, and are obtained by rewriting the balance law in conservative form. We show that the proposed scheme is well-balanced and validate the scheme for various flows given by 2×2 hyperbolic balance law. We also extend the scheme to flows on networks, particularly to include the coupling conditions at nodes of the network.

Keywords: Well-balanced scheme, discontinuous Galerkin scheme, hyperbolic balance laws, flows on networks.

1 Introduction

Many flows in nature can be modeled by nonlinear hyperbolic balance laws for e.g. gas flows given by Euler equations, shallow water equations, etc. The numerical approximations of such flows at equilibrium may introduce spurious

*E-mail: mantri@eddy.rwth-aachen.de

oscillations due to the imbalance between flux and source terms. In order to avoid this, it is necessary to design so-called well-balanced schemes which can preserve steady state of the flow and can provide non-oscillatory solutions for near-equilibrium flows. Several well-balanced schemes have been introduced in the past, for example [1, 4, 24, 25] for shallow water equations or [7, 19] for Euler equations with gravity.

A unified approach to achieve well-balancing for a general hyperbolic balance law in 1D was introduced in [11, 16]. The main idea of this approach is to rewrite the balance law in conservative form and reconstruct the so-called equilibrium variables obtained by combining the flux and source terms. The idea was then also used in [8–10, 21] for various applications in 1D and 2D using a 2nd order central upwind schemes. In the following article, we extend the approach to design high order well-balanced discontinuous Galerkin (DG) scheme for 2×2 hyperbolic balance law.

We also study flows on networks where the flow in each edge is given by a balance law along with coupling conditions at the nodes of the network. Modeling of these coupling condition could further introduce errors resulting to spurious oscillations. Several approaches to model the coupling conditions have been studied in [3, 14, 21, 26]. High order extensions of these coupling conditions have also been studied in [2, 5]. In the present article, we present a high order DG scheme which is well-balanced also on networks.

Consider Cauchy problem for hyperbolic balance law given by,

$$U_t + F(U)_x = S(U) \tag{1}$$

$$U : \mathbb{R} \times \mathbb{R}^+ \to \mathbb{R}^m, \quad F : \mathbb{R}^m \to \mathbb{R}^m, \quad S : \mathbb{R}^m \to \mathbb{R}^m \tag{2}$$

with initial conditions given by,

$$U(x, 0) = U_0(x). \tag{3}$$

Here, we consider the example of isothermal Euler equations,

$$U = \begin{bmatrix} \rho \\ q \end{bmatrix}, \; F(U) = \begin{bmatrix} q \\ \frac{q^2}{\rho} + p(\rho) \end{bmatrix}, \; S(U) = \begin{bmatrix} 0 \\ s(\rho, q) \end{bmatrix}. \tag{4}$$

where ρ is density, q is momentum and $p(\rho) = \kappa\rho^\gamma$ is pressure of gas. The equations (4) can also be used to model shallow water equations, where ρ is height of water channel, q is momentum and $p(\rho) = \frac{g}{2}\rho^2$ where g is acceleration due to gravity.

At first, we reformulate the balance law in conservative form as done in [11, 16] i.e. the balance law can be written as,

$$U_t + V_x = 0 \tag{5}$$

where V are the equilibrium variables given by,

$$V = F(U) + R(U, x) \tag{6}$$

and $R(U, x)$ is the non-local spatial integration of the source term given by,

$$R(U, x) = -\int_{x_0}^{x} S(U(\xi))d\xi. \tag{7}$$

Note that at equilibrium, the equilibrium variables, V are constant in space and time.

2 Discontinuous Galerkin scheme

DG schemes introduced by Cockburn and Shu [12, 13] have been popularly used for high order approximations of hyperbolic balance and conservation laws. The DG scheme approximates the weak form of (1),

$$\int_{\Omega_k} U_t \phi dx - \int_{\Omega_k} F(U)\phi_x dx + \mathcal{F}_{k+\frac{1}{2}}\phi_{k+\frac{1}{2}} - \mathcal{F}_{k-\frac{1}{2}}\phi_{k-\frac{1}{2}} = \int_{\Omega_k} S(U)\phi dx. \tag{8}$$

by a polynomial solution for the conservative variables, U given by,

$$U(t, x) = \sum_{i=0}^{p} U_{i,k}(t)\psi_i(x) \tag{9}$$

where $\phi \in \mathbb{P}^p(\Omega_k)$ is a test function in space of polynomials of order p, $\psi_i(x)$ is a polynomial basis function, $\mathcal{F}_{k+\frac{1}{2}}$ denotes the Riemann flux at cell boundary $x_{k+\frac{1}{2}}$ and $\Omega_k \in [x_{k-1/2}, x_{k+1/2}]$ refers to computational cell $k \; \forall \; k = 1, \ldots, N$ for total number of cells N. For a polynomial of degree p, the DG scheme gives $(p + 1)$-th order solution for the conservative variables.

2.1 DG scheme in terms of equilibrium variables

The exact solution written in conservative variables U need not be polynomial at equilibrium. Hence the projection of the equilibrium solution onto the space of piecewise polynomials introduces errors into the scheme. In addition, the flux and source terms could be highly nonlinear functions and approximation of these terms could result to an imbalance resulting to spurious oscillations in the solution at equilibrium.

Instead, we propose the approximation of equilibrium variables V by a piecewise polynomial function, i.e.,

$$V(t,x) = \sum_{i=0}^{p} V_{i,k}(t)\psi_i(x). \tag{10}$$

Since V is constant in space and time, we can exactly represent the equilibrium solution of any flow of form (1). We will see later, that the integral terms of the DG scheme can also be evaluated exactly, thus resulting in preservation of the equilibrium solution over time.

Weak form of (5) can be written as,

$$\int_{\Omega_k} U_t \phi dx - \int_{\Omega_k} V\phi_x dx + V_{k+\frac{1}{2}}\phi_{k+\frac{1}{2}} - V_{k-\frac{1}{2}}\phi_{k-\frac{1}{2}} = 0 \tag{11}$$

where $\phi \in \mathbb{C}^1(\Omega)$ is a test function. Thus, using chain rule, $U_t = \frac{\partial U}{\partial V} V_t$ we get,

$$\int_{\Omega_k} \frac{\partial U}{\partial V} V_t \phi dx - \int_{\Omega_k} V\phi_x dx + V_{k+\frac{1}{2}}\phi_{k+\frac{1}{2}} - V_{k-\frac{1}{2}}\phi_{k-\frac{1}{2}} = 0. \tag{12}$$

Substituting the polynomial approximation (10) of the equilibrium variables, we get,

$$\int_{\Omega_k} \frac{\partial U}{\partial V} \sum_{i=0}^{p} [V_{i,k}(t)]_t \psi_i(x)\phi dx - \int_{\Omega_k} V\phi_x dx + V_{k+\frac{1}{2}}\phi_{k+\frac{1}{2}} - V_{k-\frac{1}{2}}\phi_{k-\frac{1}{2}} = 0 \tag{13}$$

or,

$$\sum_{i=0}^{p} \Big(\int_{\Omega_k} \frac{\partial U}{\partial V} \psi_i \phi dx \Big) [V_{i,k}(t)]_t - \int_{\Omega_k} V\phi_x dx + V_{k+\frac{1}{2}}\phi_{k+\frac{1}{2}} - V_{k-\frac{1}{2}}\phi_{k-\frac{1}{2}} = 0. \tag{14}$$

To find $p+1$ unknowns, $V_{i,k}$, we need $p+1$ basis functions $\Phi = \phi_j, j = 0, \ldots, p$, which gives,

$$\sum_{i=0}^{p} \Big(\int_{\Omega_k} \frac{\partial U}{\partial V} \psi_i \phi_j dx \Big) [V_{i,k}(t)]_t - \int_{\Omega_k} V(\phi_j)_x dx + V_{k+\frac{1}{2}}\phi_{k+\frac{1}{2}} - V_{k-\frac{1}{2}}\phi_{k-\frac{1}{2}} = 0. \tag{15}$$

or in matrix vector form,

$$M(\mathcal{V}_k)_t - \int_{\Omega_k} V\Phi_x dx + V_{k+\frac{1}{2}}\Phi_{k+\frac{1}{2}} - V_{k-\frac{1}{2}}\Phi_{k-\frac{1}{2}} = 0 \tag{16}$$

where

$$M = [M_{ij}]_{i,j=1,\ldots,p+1} \quad M_{ij} = \int_{\Omega_k} \frac{\partial U}{\partial V} \psi_i \phi_j dx \tag{17}$$

and

$$\mathcal{V}_k = [V_i]_{i=0,\ldots,p} \tag{18}$$

$$\Phi = [\phi_j]_{j=0,\ldots,p}. \tag{19}$$

The ODE for $\mathcal{V}_k$ in equation (16) can be solved using SSP Runge-Kutta schemes as given in [13]. The time evolution for $\mathcal{V}_k$ using a third-order time discretization is given by,

$$\begin{aligned} V_k^{(1)} &= \mathcal{V}_k^n + \Delta t^n L(\mathcal{V}_k^n) \\ V_k^{(2)} &= \frac{3}{4} V_k^n + \frac{1}{4} V_k^{(1)} + \frac{1}{4} \Delta t^n L(V_k^{(1)}) \\ \mathcal{V}_k^{(n+1)} &= \frac{1}{3} V_k^n + \frac{2}{3} V_k^{(2)} + \frac{2}{3} \Delta t^n L(V_k^{(2)}) \end{aligned} \tag{20}$$

where $L(V_k) = M(V_k)^{-1} \left(\int_{\Omega_k} V \Phi_x dx - V_{k+\frac{1}{2}} \Phi_{k+\frac{1}{2}} + V_{k-\frac{1}{2}} \Phi_{k-\frac{1}{2}} \right)$ and Δt^n is the numerical time-step calculated using *cfl*-condition.

Note, that since the equilibrium variables and the test function are polynomials, the integral $\int_{\Omega_k} V \Phi_x dx$ can be computed exactly using Gaussian quadrature with sufficient number of quadrature points. For a $(p+1)$-th order DG scheme, we require p quadrature points with Gauss-Legendre quadrature or $p+1$ quadrature points with Gauss-Lobatto quadrature.

Theorem 2.1. *The semi-discrete discontinuous Galerkin (DG) scheme given in* (16) *with fluxes on cell-boundaries given by a consistent approximate Riemann solver, preserves equilibrium solution of flows given by* (1).

Proof. To prove the theorem, we start by assuming that the flow is at equilibrium at time-step, t^n i.e. $V(x, t^n) = V^*$ and prove that the scheme preserves the equilibrium solution for time t^{n+1} i.e. $V(x, t^{n+1}) = V^*$. Thus, we need to show that $\mathcal{V}_t = 0$ or from (16),

$$- \int_{\Omega_k} V \Phi_x dx + V_{k+\frac{1}{2}} \Phi_{k+\frac{1}{2}} - V_{k-\frac{1}{2}} \Phi_{k-\frac{1}{2}} = 0. \tag{21}$$

The equilibrium variables, V at cell interfaces can be calculated using a consistent approximate Riemann solver, $V_{k+\frac{1}{2}}(V, V) = V$, for example,

$$V_{k+\frac{1}{2}} = \frac{a^+_{k+\frac{1}{2}} V^-_{k+\frac{1}{2}} - a^-_{k+\frac{1}{2}} V^+_{k+\frac{1}{2}}}{a^+_{k+\frac{1}{2}} - a^-_{k+\frac{1}{2}}} + \frac{a^+_{k+\frac{1}{2}} a^-_{k+\frac{1}{2}}}{a^+_{k+\frac{1}{2}} - a^-_{k+\frac{1}{2}}} (U(V^+_{k+\frac{1}{2}}, R^+_{k+\frac{1}{2}}) - U(V^-_{k+\frac{1}{2}}, R^-_{k+\frac{1}{2}})). \tag{22}$$

Note that the only difference compared to standard Riemann solvers is that, given equilibrium variables on the cell boundaries, we calculate the conservative variables from the solution of equilibrium variables, instead of the contrary. When the source term, $s(U)$ is bounded, the integral over the cell boundaries is a zero measure and hence we get $\int_{x^-_{k+\frac{1}{2}}}^{x^+_{k+\frac{1}{2}}} s(U)dx = 0$ or $R^+_{k+\frac{1}{2}} = R^-_{k+\frac{1}{2}} = R_{k+\frac{1}{2}}$.

It has been shown in [21], that $U : \mathbb{R}^2 \times \mathbb{R} \rightarrow \mathbb{R}^2$ has unique solution for flux of the form in (4), when the flow is away from sonic point. Therefore as $V^+_{k+\frac{1}{2}} = V^-_{k+\frac{1}{2}} = V^*$ at equilibrium and the integral of source term is continuous, we get,

$$U(V^+_{k+\frac{1}{2}}, R^+_{k+\frac{1}{2}}) = U(V^-_{k+\frac{1}{2}}, R^-_{k+\frac{1}{2}}).$$

The computation of U from V for equations (4) is given in Remark 2.2. Hence, the first term of (22) reduces to V^* and the second term goes to zero at equilibrium, giving $V_{k-\frac{1}{2}} = V_{k+\frac{1}{2}} = V^*$.

Substituting the equilibrium solution for V in (21), we are left with divergence theorem for the test function, $-\int_{\Omega_k} \Phi_x dx + \Phi_{k+\frac{1}{2}} - \Phi_{k-\frac{1}{2}} = 0$. Since the integral $\int_{\Omega_k} V\Phi_x dx$ can be evaluated exactly using Gaussian quadrature, the divergence theorem can be solved exactly and hence the scheme is well-balanced. □

Remark 2.2. *For Euler equations* (4)*, the density, ρ can be calculated from the equilibrium variables, $V = (q, K)^T$ with pressure $p(\rho) = \kappa\rho^\gamma$ by solving a nonlinear equation given by*

$$\kappa\rho^{\gamma+1} - (K - R)\rho + q^2 = 0.$$

The solution to these equations is unique when the flow is away from the sonic point as has been shown in [21]. For $\gamma = 1$, the equation reduces to a quadratic equation whose roots correspond to subsonic and supersonic flow. The solution of the cubic polynomial for $\gamma = 2$ is calculated as given in [8] for the examples of shallow water equations.

The global integral of the source term, R is computed point-wise between each quadrature point. At first, we fix a starting point $\hat{x}$ for the integration such that $R(\hat{x}) = 0$. The integral, R^k_{j+1} at the quadrature point x_{j+1} in cell k can be then computed recursively from the solution at point x_j. Using Taylor series expansion about point x_j we can calculate R^k_{j+1} as,

$$\begin{aligned} R^k_{j+1} &= R^k_j + (R_x)^k_j \Delta x_j + (R_{xx})^k_j \frac{\Delta x_j^2}{2} + \dots \\ R^k_{j+1} &= R^k_j - s^k_j \Delta x_j - (s_x)^k_j \frac{\Delta x_j^2}{2} - \dots, \end{aligned} \tag{23}$$

since $R_x = -s$ and where $\Delta x_j = x_{j+1} - x_j$.

The source term and the first p spatial derivatives at point j can be computed from the solution of equilibrium variable and the lower order derivatives of s. Furthermore, as mentioned earlier R is assumed to be continuous at the cell interfaces for continuous and bounded source terms, $s(U)$.

2.2 Discussion on the well-balanced scheme

The application of chain rule in (12), helps obtain a linear system of equations for the variables $\mathcal{V}_t$. However, this does not guarantee the mass conservation of the scheme numerically for flows away from equilibrium. From the numerical experiments, we observed that though this error could indeed be observed for some examples, it is smaller than the truncation error of the DG scheme. Moreover, we have checked that the scheme computes shock speeds correctly.

The concept of change of variables was also used in a series of papers of Hughes' and collaborators [18], who transform the Euler equations into a symmetric hyperbolic system using the framework of Godunov [17] and Mock [22]. For this change of variables, $U'(V)$ becomes the Hessian of an entropy function, which is a positive definite matrix. This yields a space time DG scheme which satisfies a discrete entropy inequality. It is instructive to have a look at DG schemes formulated in entropy, equilibrium and the standard conservative variables. Each of these schemes have their advantages but do not satisfy all the properties simultaneously: the standard scheme is conservative in all variables; the scheme of Hughes et.al. guarantees an entropy inequality; and our scheme is well-balanced by construction. Each scheme needs to be refined to obtain the other properties.

Besides using a different transformation $U(V)$, there is another difference in the time discretization. While we invert the mass matrix $M(V)$ in (12) and use the Runke-Kutta steps (20), Hughes and coauthors discretize (12) using a space-time DG scheme. This leads to nonlinear equations for the coefficients of entropy variables. It would be interesting to derive a space-time DG scheme based on equilibrium variables and see if this reduces the mass error.

Remark 2.3. *Compared to the standard DG scheme, the above scheme* (16) *is computationally more expensive due to the inversion of the mass matrix, M. In the standard DG scheme, ψ and ϕ can be chosen such that they are orthogonal to each other i.e., $\int_\Omega \psi_i \phi_j = \delta_{ij}$, where δ_{ij} is Kronecker delta; resulting to an identity matrix as mass matrix. In general for the well balanced scheme, the test and basis functions can be made orthogonal with respect to only some of the terms of the mass matrix, for instance we can choose ψ and ϕ such that $\int_\Omega \frac{\partial U_k}{\partial V_l} \psi_i \phi_j = \delta_{ij}$ for some choice of $k, l = 1, 2$, but not for all k, l.*

We also tried to obtain a test function which simplifies the mass matrix. However this could affect the well-balancing property of the scheme, since equation (21) will not be satisfied numerically.

Remark 2.4. *The DG scheme* (16) *can be simplified further for Euler equations* (4) *to the form,*

$$(\mathcal{U}_k^{(2)})_t - \int_{\Omega_k} K\Phi_x dx + K_{k+\frac{1}{2}}\Phi_{k+\frac{1}{2}} - K_{k-\frac{1}{2}}\Phi_{k-\frac{1}{2}} = 0 \tag{24}$$

$$M^{(2)}(\mathcal{K}_k)_t - \int_{\Omega_k} U_2\Phi_x dx + (U_2)_{k+\frac{1}{2}}\Phi_{k+\frac{1}{2}} - (U_2)_{k-\frac{1}{2}}\Phi_{k-\frac{1}{2}} - M^{(1)}(\mathcal{U}_k^{(2)})_t = 0 \tag{25}$$

where $\mathcal{V} = (\mathcal{U}^{(2)}, \mathcal{K})^T$ *and,*

$$M^{(1)} = \Big[\int_{\Omega_k} \frac{\partial U_1}{\partial U_2}\psi_i\phi_j dx\Big]_{i,j=1,\ldots,p+1}, \quad M^{(2)} = \Big[\int_{\Omega_k} \frac{\partial U_1}{\partial K}\psi_i\phi_j dx\Big]_{i,j=1,\ldots,p+1},$$

so as to increase the computational efficiency of the scheme. The scheme now requires inversion of a matrix $M^{(2)}$ *of dimension* $p \times p$ *as compared to the matrix* M *of dimensions* $2p \times 2p$.

We observed that for the numerical experiments in Section 3 and Section 4, the inversion of the mass matrices $M^{(2)}$ took about 25-30% of the total run-time of our code.

3 Numerical Tests

In the following Section, we test the numerical scheme discussed in Section 2 for higher order convergence and well-balancing of shallow water equations and isothermal Euler equations. The scheme is compared with the standard (non-well-balanced) DG scheme proposed by Cockburn and Shu [13]. In the following numerical tests, both the well-balanced and non-well-balanced DG scheme are third order accurate. The computational domain for the tests is $\Omega = [0, 1]$ and the tests are run with *cfl* number = 0.2.

3.1 Shallow water equations

Consider shallow water equations of the form (4) with ρ, q denoting height and momentum of water respectively, with source term given by,

$$s(\rho, q) = -g\rho b_x - \nu\frac{q|q|}{\rho^{7/3}} \tag{26}$$

where $b(x)$ stands for bottom topography and ν is the friction coefficient.

3.1.1 Convergence test

At first, we check the order of convergence of the well-balanced DG scheme for a standard test problem for shallow water equations considered in [25]. The initial conditions for height and momentum are given by,

$$\rho(x,0) = 5 + e^{\cos(2\pi x)},$$
$$q(x,0) = \sin(\cos(2\pi x))$$

and bottom topography,$b(x)$ is given by,

$$b(x) = \sin^2(\pi x) \tag{27}$$

and $\nu = 0$. We compare the solution of the well-balanced DG scheme for number of cells, $N = 20, 40, 80, 160$ with a reference solution calculated with $N = 1600$. The L_1 errors for the equilibrium variable at $T = 0.1$ are as given in Table 1.

No. of cells	$\|\|q - q^*\|\|_{L_1}$	order	$\|\|K - K^*\|\|_{L_1}$	order
20	1.3677×10^{-2}		1.4667×10^{-1}	
40	2.2571×10^{-3}	2.60	1.8432×10^{-2}	2.99
80	2.0125×10^{-4}	3.48	1.6561×10^{-3}	3.47
160	1.7087×10^{-5}	3.55	1.4802×10^{-4}	3.48

Table 1: L_1 errors at time $T = 0.1$ with $N = 20, 40, 80, 160$ computed by the well-balanced DG scheme with bottom topography given by (27)

As can be observed from Table 1, the well-balanced DG scheme along with SSP Runge Kutta method in time, preserves third order accuracy of the solution. The errors and convergence rates of the non-well-balanced DG scheme are comparable to those of the well-balanced DG scheme.

3.1.2 Steady state

We now test the well-balancing property of the scheme for steady state flow given by constant equilibrium variables. Consider a moving water steady state where the initial conditions are given by $q(x, t = 0) = 0.1$ and $K(x, t = 0) = \frac{g\rho^2}{2} + \int g\rho b_x dx = 0.4$ with bottom topography, $b(x) = 0.1e^{-100(x-0.5)^2}$ and friction factor, $\nu = 0.2$. The L_1 errors for the well-balanced and non-well-balanced scheme at $T = 1$ are as in Table 2.

We see from the results in Table 2, that the scheme preserves the steady state exactly up to machine precision, which is not the case with the non-well-balanced scheme.

	$\|\|q - q^*\|\|_{L_1}$		$\|\|K - K^*\|\|_{L_1}$	
No. of cells	WB	NWB	WB	NWB
20	1.304×10^{-15}	2.534×10^{-4}	3.450×10^{-15}	8.602×10^{-4}
40	3.128×10^{-16}	6.238×10^{-5}	9.419×10^{-16}	2.124×10^{-4}
80	8.623×10^{-16}	1.538×10^{-5}	2.424×10^{-16}	5.304×10^{-5}

Table 2: Comparison of L_1 errors between well-balanced (WB) and non-well-balanced (NWB) scheme for moving water steady state at time T=1

3.1.3 Perturbation to steady state

We now test the behavior of the well-balanced and standard DG scheme for flows which are near steady state. Consider initial conditions for height of water and momentum given by $q(x,t=0) = 0.1$ and $\rho(x,t=0) = \rho^*(x) + 0.01e^{-1000(x-0.4)^2}$ with bottom topography $b(x) = 0.1e^{-400(x-0.6)^2}$ and where $\rho^*(x)$ is the equilibrium solution calculated with $K^* = 0.4$ and $q^* = 0.1$. The results for height of water at $T = 0.2$ are as given in Figure 1.

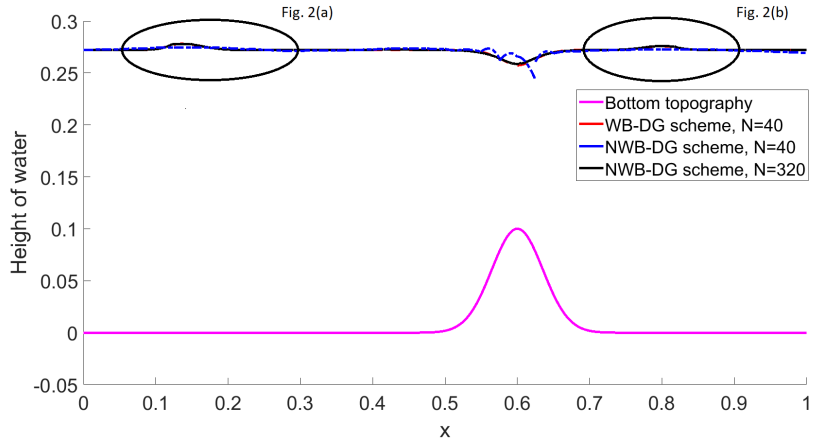

Figure 1: Solution for surface level of water at time, $T = 0.2$ with bottom topography for perturbation to equilibrium state

One can see from the results in Figure 1, that the solution with the standard DG scheme does not capture the perturbation accurately with a coarse grid of $N = 40$. On the other hand, the well-balanced scheme is able to capture the perturbations accurately even with a coarse grid of $N = 40$ and the results are comparable to the solution obtained by the standard DG scheme with $N = 320$. Also, we see that the perturbed wave passes over the bump in bottom topography without distorting the solution.

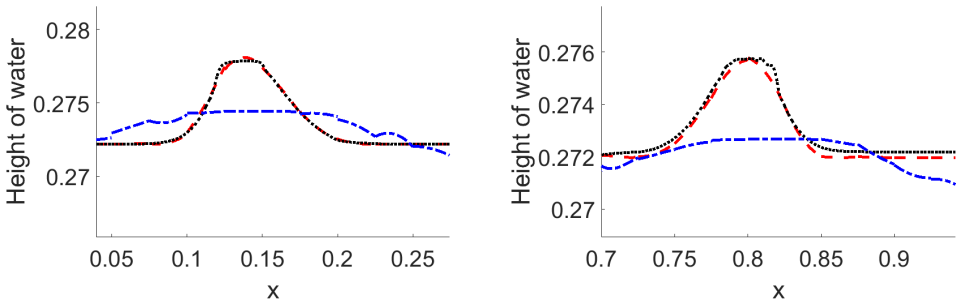

(a) Zoomed view of the first traveling wave in Figure 1

(b) Zoomed view of the second traveling wave in Figure 1

Figure 2: Zoomed view of the perturbations in the water surface in Figure 1.

3.2 Gas flow in pipes

Next, we test the well-balanced scheme for gas flow in pipes given by isothermal Euler equations (4), with source term,

$$s(\rho, q) = -\frac{f_g}{2D}\frac{q|q|}{\rho}, \tag{28}$$

and pressure $p(\rho) = a^2\rho$, where a is speed of sound, D is diameter of the pipe and f_g is the friction coefficient due to wall-friction within the pipes.

3.2.1 Steady state

At first, we test the well-balancing property of the scheme for the Euler equations (4). The initial conditions for the equilibrium variables are given by $q(x, t = 0) = q^* = 0.1$ and $K(x, t = 0) = K^* = \frac{q^2}{\rho} + a^2\rho + \int \frac{f_g}{2D}\frac{q|q|}{\rho}dx = 0.4$ with $a = 1$ and $\frac{f_g}{2D} = 1$. The L_1 errors for the well-balanced and non-well-balanced DG schemes at $T = 1$ are as given in 3.

	$\|\|q - q^*\|\|_{L_1}$		$\|\|K - K^*\|\|_{L_1}$	
No. of cells	WB	NWB	WB	NWB
20	2.925×10^{-16}	1.312×10^{-8}	8.593×10^{-16}	8.476×10^{-9}
40	1.526×10^{-17}	1.639×10^{-9}	9.946×10^{-18}	1.072×10^{-9}
80	1.584×10^{-17}	2.503×10^{-10}	7.748×10^{-18}	1.344×10^{-10}

Table 3: Comparison of L_1 errors between well-balanced (WB) and non-well-balanced (NWB) scheme for gas flow at steady state at time T=1

Similar to the case of shallow water equations, the well-balanced DG scheme is able to preserve steady state of the flow exactly up to machine precision unlike the standard non-well-balanced scheme.

3.2.2 Perturbation to steady state & Convergence test

Now consider perturbation in momentum for the isothermal Euler equations. The initial condition for equilibrium variables are $q = q^*(1 + \eta e^{-100(x-0.5)^2})$, $K = K^*$ where q^*, K^* are same as previous example. We now check the order of convergence of the scheme with $N = 20, 40, 80, 160$ with $a = 1$, $\frac{f_g}{2D} = 1$ and $\eta = 10^{-3}$. The solution is compared with reference solution generated with $N = 1600$. The L_1 errors for the equilibrium variables at $T = 0.2$ are as given in Table 4.

No. of cells	$\|\|q - q^*\|\|_{L_1}$	order	$\|\|K - K^*\|\|_{L_1}$	order
20	2.648×10^{-8}		2.331×10^{-8}	
40	3.169×10^{-9}	3.06	2.756×10^{-9}	3.08
80	4.002×10^{-10}	2.99	3.489×10^{-10}	2.98
160	4.973×10^{-11}	3.01	4.344×10^{-11}	3.01

Table 4: L_1 errors at time $T = 0.2$ with $N = 20, 40, 80, 160$ computed by the well-balanced DG scheme

We can see from the results in Table 4, that the well-balanced DG scheme provides accurate order of convergence, for the example of gas flow with friction as well.

We now compare the solution of the well-balanced DG scheme with standard DG scheme for perturbation, $\eta = 10^{-7}$. Figure 3 shows the results for momentum at time, $T = 0.2$ with the well-balanced and standard DG scheme.

As can be seen from the results in Figure 3, the solution of the well-balanced DG scheme with $N = 40$ is almost the same as that of the non-well-balanced DG scheme with $N = 320$. Whereas for non-well balanced scheme with $N = 40$ the solution is distorted and does not capture the perturbation accurately.

4 Flows on networks

In the following section, we extend the DG scheme to flows on networks wherein in addition to the balance law within each edge of the network, we need coupling conditions at the node of a network. For literature on coupling conditions for

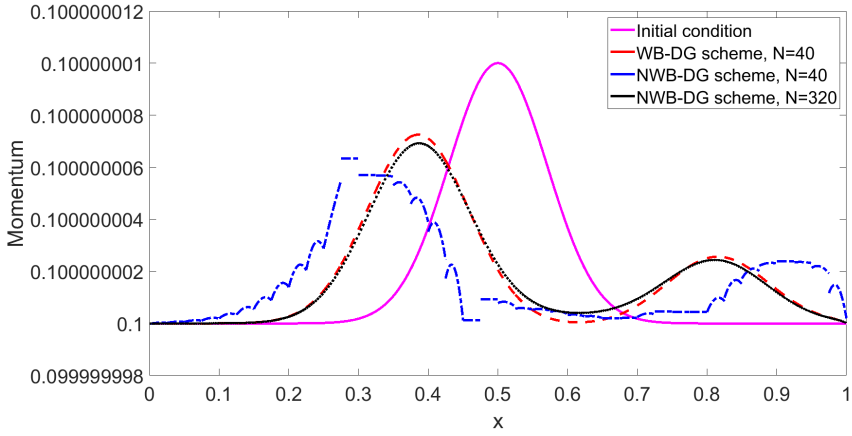

Figure 3: Solution for momentum of water at $T = 0.2$ for initial condition given by perturbation to steady state

flows in network, see [3, 6, 14, 23]. In [21], we have shown that the solution of the coupling conditions computed from the equilibrium variables, results in a well-balanced scheme at the node along with a second order central upwind scheme along the edges. Solving the coupling conditions in the same manner at each Runge-Kutta stage preserves the order of the DG scheme. In this section, we summarize the method used in [21].

Consider a node connected to M pipes at a junction, O at x_0. The gas flow within pipe j $\forall j = 1, \dots M$ is given by,

$$(U_j)_t + (V_j)_x = 0 \tag{29}$$

with boundary conditions at the node given implicitly by the coupling conditions,

$$\theta(U_1^*(x_0,t), \dots, U_N^*(x_0,t)) = 0 \quad t \geq 0, \quad \theta : \mathbb{R}^{2M} \to \mathbb{R}^M. \tag{30}$$

The solution U_i^* at the node is connected to the interior solution within the pipe, U_i^0 through the incoming Lax curves at the node x_0. The corresponding equilibrium variables are denoted by V_i^* and V_i^0 respectively. For construction of Lax curves, see [15, 20]. In this paper, we restrict ourselves to subsonic flow, i.e. $\lambda_1 < 0 < \lambda_2$. This implies that the first family of Lax curves, denoted by $\mathcal{L}_1(U^0, \sigma)$, enters the incoming pipe and the second family of Lax curves, $\mathcal{L}_2(U^0, \sigma)$ enters the outgoing pipes at the node, as shown in Figure 4. Note that, we need to consider the forward Lax curves for the incoming pipes and the backward Lax curves for the outgoing pipes. Thus in order to compute the solution at the node, we need to find the parameters σ_i within each pipe from the coupling conditions at the node.

$$\theta(\mathcal{L}_1(U_i^0, \sigma_i), \mathcal{L}_2(U_j^0, \sigma_j)) = 0 \quad \forall i \in I^-, j \in I^+. \tag{31}$$

Here I^- refers to the set of incoming pipes and I^+ refers to the set of outgoing pipes.

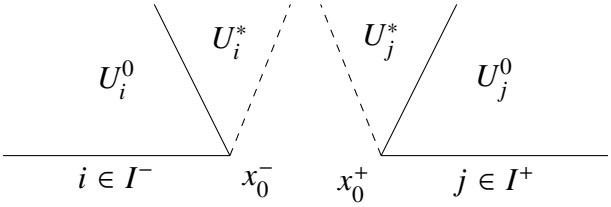

Figure 4: 1-wave entering incoming pipe and 2-wave entering outgoing pipe for subsonic flow

In order to obtain a well-balanced solution at the node, we reformulate the coupling conditions in terms of the equilibrium variables V_i as has been done in [21]. The solution at the node $V_i^* = \mathcal{L}_1(V_i^0, R_i^0, \sigma_i) \forall i \in I^-$ or $V_j^* = \mathcal{L}_2(V_j^0, R_j^0, \sigma_j) \forall j \in I^+$ can be computed by solving the coupling conditions,

$$\Theta(V_i^*(\sigma_i), R_i^*) = 0 \quad i \in I^- \cup I^+, \quad \Theta : \mathbb{R}^{2M} \times \mathbb{R}^M \to \mathbb{R}^M. \tag{32}$$

to find the parameter σ_i where $R_i^* = R_i^0$. The well-posedness of these coupling conditions at the node has been shown in [21].

Alternatively, one could also use ADER type schemes for calculating the solution in time within each edge of the network. In that case, we need to calculate higher order coupling conditions to preserve the high order accuracy at the node. Higher order coupling conditions have been studied in [2, 5]. Using the same strategy in terms of the equilibrium variables, leads to well-balanced coupling conditions.

Since the coupling conditions are satisfied at all times, we take $\frac{\partial^i \Theta(V_i(\sigma_i), R_i)}{\partial t^i} = 0 \forall i = 0, \ldots, p$, from which we can evaluate $\frac{\partial^i V}{\partial t^i}$. The equilibrium variables are then approximated using a Taylor series expansion, $V(t^n + \tau) = V(t^n) + \frac{\partial V}{\partial t}\tau + \frac{\partial^2 V}{\partial t^2}\frac{\tau^2}{2} + \ldots$. It can easily be checked that the solution to higher order time derivatives of the coupling condition results in $\frac{\partial^i V}{\partial t^i} = 0 \, \forall i = 0, \ldots, p$, when the flow is at equilibrium i.e. $V(x,t) = V^*$ leading to well-balanced solution at the node.

4.1 Numerical examples

We now test the coupling conditions for flows on network of hyperbolic balance laws. The coupling conditions at the nodes of the network are solved using Newtons iteration with initial conditions for Newtons iteration given by the old traces in each pipe.

4.1.1 Network of water channels

Consider network given in Figure 5, wherein flow in each edge is given by shallow water equation with coupling condition, $\Theta(V_i, R_i)$ given by,

$$\Theta(V_i(\sigma_i), R_i) = \begin{bmatrix} \sum_{i\in I^-} w_i\rho(q_i, K_i)q_i - \sum_{j\in I^+} w_j\rho(q_j, K_j)q_j \\ \rho(q_1, K_1) - \rho(q_2, K_2) \\ \vdots \\ \rho_(q_{M-1}, K_{M-1}) - \rho_(q_M, K_M) \end{bmatrix} \tag{33}$$

where w_i denotes the width of the water channel and $V_i = (q_i, K_i)^T$. The first coupling condition represents mass balance at the node and the other $M - 1$ coupling conditions stand for continuity of water surface at the node.

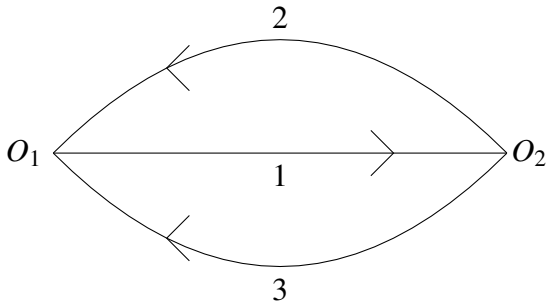

Figure 5: Test problem for network of network of water channels

Order of convergence At first we test the order of convergence of the scheme on the network, with initial condition given by,

$$\begin{aligned} \rho_i(x, 0) &= 5 + e^{\cos(2\pi x)} \,\forall\, i = 1, 2, 3, \\ q_1(x, 0) &= \sin(\cos(2\pi x)) \\ q_2(x, 0) &= q_3(x, 0) = -0.5\sin(\cos(2\pi x)) \end{aligned}$$

and the bottom topography given by,

$$b_i(x) = \sin^2(\pi x).$$

The width of all the channels, $w_1 = w_2 = w_3 = 1$. The L_1 error for the equilibrium variables at time $T = 0.1$ is as given in Table 5.

We can see from Table 5, that we obtain the expected order of convergence of the DG scheme, and the order is not affected due to the solution of the coupling conditions at the node.

No. of cells	$\|\|q - q^*\|\|_{L_1}$	order	$\|\|K - K^*\|\|_{L_1}$	order
20	4.191×10^{-2}		4.452×10^{-1}	
40	6.502×10^{-3}	2.688	5.652×10^{-2}	2.977
80	5.694×10^{-4}	3.513	5.037×10^{-3}	3.488
160	6.634×10^{-5}	3.101	5.932×10^{-4}	3.085

Table 5: L_1 errors at time $T = 0.1$ with $N = 20, 40, 80, 160$ computed by the well-balanced DG scheme for a network of water channels given in Figure 5

Flow near steady state on a network We now test the scheme for a flow given by perturbation to the lake at rest steady state on the network in Figure 5. We add a perturbation to the height of water surface and track the perturbation over time. The initial condition is given by,

$$\rho_1(x, t = 0) = \rho(q_1^*, K_1^*) + 10^{-2} e^{-100(x-0.5)^2},$$
$$\rho_2(x, t = 0) = \rho(q_2^*, K_2^*), \quad \rho_3(x, t = 0) = \rho(q_3^*, K_3^*)$$

where equilibrium variables $q_i^* = 0$ and $K_i^* = 1$, $\forall\, i = 1, \ldots, N$ and bottom topography,

$$b_1(x) = 0,\ b_2(x) = 0.1 e^{-400(x-0.75)^2},\ b_3(x) = 0.1 e^{-400(x-0.25)^2}.$$

Figure 6 shows the solution for the height of water surface along the three edges at time $T = 0, 0.3, 0.5$ with $N = 40$,

From Figure 6 at time $T = 0.3$, we see that the perturbed wave passes smoothly through the junction and is partially reflected back without being distorted. We also see that at time $T = 0.5$, the wave has also passed through the bump in bottom topography in edges 2,3.

The small undulations in the solution of water surface where there is non-zero bottom topography are due to the definition of the discrete steady state, given by constant equilibrium variables, resulting in effect of the higher order terms of the bottom topography on the water surface; and are not introduced by the DG scheme over time. These errors due to the bottom topography can be reduced by considering more quadrature points to calculate R using equation (23). Comparison of the discrete steady state solution for edge 2 with additional quadrature points is as shown in Figure 7.

4.1.2 Network of gas-pipelines

Consider a network of gas pipelines as given in Figure 8. The flow within each pipe of the network is given by isothermal Euler equations (4) with $p(\rho) = \rho$ and source

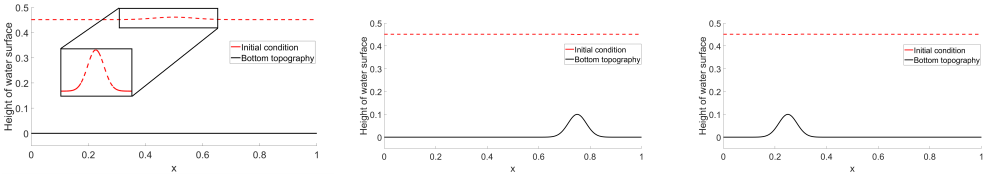

(a) Channel 1 at $T = 0$ (b) Channel 2 at $T = 0$ (c) Channel 3 at $T = 0$

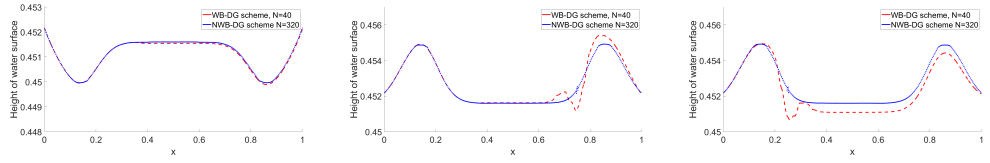

(d) Channel 1 at $T = 0.3$ (e) Channel 2 at $T = 0.3$ (f) Channel 3 at $T = 0.3$

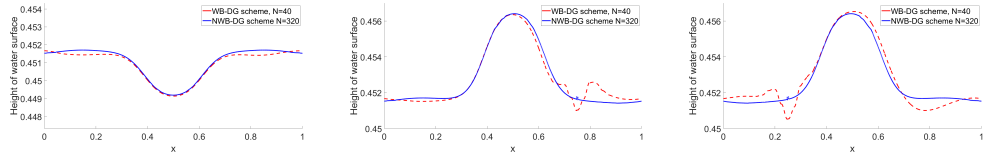

(g) Channel 1 at $T = 0.5$ (h) Channel 2 at $T = 0.5$ (i) Channel 3 at $T = 0.5$

Figure 6: Solution of water surface (red) at time, $T = 0, 0.3, 0.5$ for a perturbed equilibrium state for the network given in Figure 5.

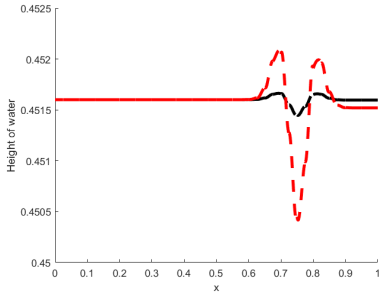

Figure 7: Discrete steady state solution in edge 2 with 4 quadrature points (in red) and 10 quadrature points (in black) in each cell to calculate R using (23).

term given by friction in pipes as given in (28). At the node of the network we use the coupling condition of mass-balance and continuity of pressure, described in [3], and are given by,

$$\Theta(V_i(\sigma_i), R_i) = \begin{bmatrix} \sum_{i\in I^-} A_i q_i - \sum_{j\in I^+} A_j q_j \\ P(q_1, K_1) - P(q_2, K_2) \\ \vdots \\ P(q_{M-1}, K_{M-1}) - P(q_M, K_M) \end{bmatrix} \tag{34}$$

where A_i is the cross-sectional area of pipe i at the node and $P(q, K)$ denotes pressure written in terms of the equilibrium variables.

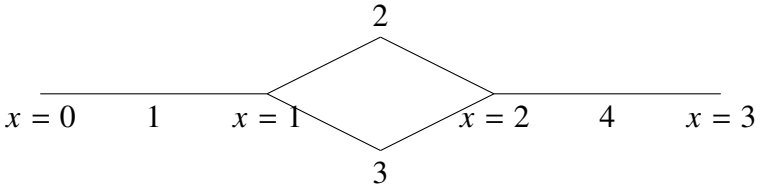

Figure 8: Test problem for network of gas-pipeline

Perturbation to steady state In the following test, we add a perturbation to the momentum at equilibrium in Pipe 2. The initial conditions for this flow are given by,

$$q_1 = q_4 = 0.1, \quad q_3 = 0.05, \quad q_2 = 0.05(1 + 10^{-7} e^{-100(x-1.5)^2})$$
$$K_1 = 0.4, \quad K_2 = K_3 = 0.3502, \quad K_4 = 0.3652.$$

The initial conditions are selected in such a way the solution satisfies the coupling conditions and hence no additional wave is generated from the node. The initial condition and solution at $T = 1$ for momentum are as given in Figure 9.

We can see from the results in Figure 9 that the initial perturbation in Pipe 2 moves through the nodes at $x = 1$ and $x = 2$ to Pipe 1/Pipe 3 and Pipe 4/Pipe 3 respectively; and is partially reflected back to Pipe 2. Note that there are no spurious oscillations that are introduced either due to the imbalance between flux and source or due to the coupling conditions at the node, thus confirming the well-balanced property of the scheme.

Conclusion

In this article, we have designed a well-balanced discontinuous Galerkin scheme of high order accuracy which can preserve steady states exactly for subsonic

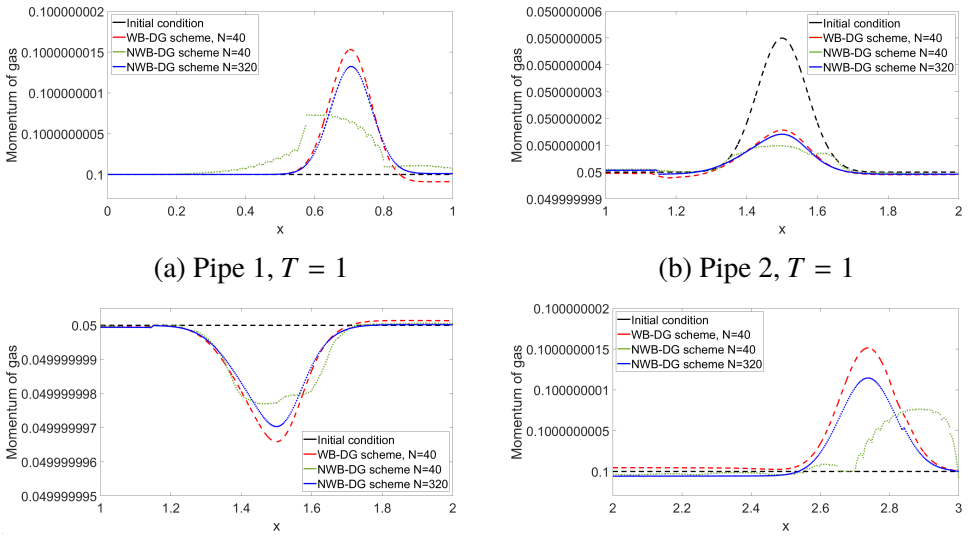

(a) Pipe 1, $T = 1$

(b) Pipe 2, $T = 1$

(c) Pipe 3, $T = 1$

(d) Pipe 4, $T = 1$

Figure 9: Solution for momentum of gas at $T = 1$ for network in Figure 8

flow for a general hyperbolic balance law of form (1). In particular, we test the scheme for shallow water equation and isothermal Euler equations. We also see that the scheme can capture perturbations of steady states accurately and provide solutions which are similar to that of standard DG scheme with a finer mesh. The application of the scheme to flows on networks also shows that the scheme can capture perturbations accurately across the node of the network, while also providing high order accuracy of the DG scheme.

Acknowledgments

This work has been supported by Deutsche Forschungsgemeinschaft (DFG, German Research Foundation) – Projektnummer 320021702/GRK2326 – Energy, Entropy, and Dissipative Dynamics (EDDy). The authors would like to thank Michael Herty for his insights and expertise that greatly assisted the research.

References

[1] E. Audusse, F. Bouchut, M.-O. Bristeau, R. Klein, and B. t. Perthame, *A fast and stable well-balanced scheme with hydrostatic reconstruction for shallow water flows*, SIAM J. Sci. Comput., 25 (2004), pp. 2050–2065.

[2] M. K. Banda, A.-S. Häck, and M. Herty, *Numerical discretization of coupling conditions by high-order schemes*, J. Sci. Comput., 69 (2016), pp. 122–145.

[3] M. K. Banda, M. Herty, and A. Klar, *Coupling conditions for gas networks governed by the isothermal Euler equations*, Netw. Heterog. Media, 1 (2006), pp. 295–314.

[4] A. Bollermann, G. Chen, A. Kurganov, and S. Noelle, *A well-balanced reconstruction of wet/dry fronts for the shallow water equations*, J. Sci. Comput., 56 (2013), pp. 267–290.

[5] R. Borsche and J. Kall, *ADER schemes and high order coupling on networks of hyperbolic conservation laws*, J. Comput. Phys., 273 (2014), pp. 658–670.

[6] A. Bressan, S. Čanić, M. Garavello, M. Herty, and B. Piccoli, *Flows on networks: recent results and perspectives*, EMS Surv. Math. Sci., 1 (2014), pp. 47–111.

[7] P. Chandrashekar and C. Klingenberg, *A second order well-balanced finite volume scheme for Euler equations with gravity*, SIAM J. Sci. Comput., 37 (2015), pp. B382–B402.

[8] Y. Cheng, A. Chertock, M. Herty, A. Kurganov, and T. Wu, *A new approach for designing moving-water equilibria preserving schemes for the shallow water equations*, J. Sci. Comput., 80 (2019), pp. 538–554.

[9] A. Chertock, S. Cui, A. Kurganov, c. N. Özcan, and E. Tadmor, *Well-balanced schemes for the Euler equations with gravitation: conservative formulation using global fluxes*, J. Comput. Phys., 358 (2018), pp. 36–52.

[10] A. Chertock, M. Dudzinski, A. Kurganov, and M. Lukáčová-Medviďová, *Well-balanced schemes for the shallow water equations with Coriolis forces*, Numer. Math., 138 (2018), pp. 939–973.

[11] A. Chertock, M. Herty, and S. N. Özcan, *Well-balanced central-upwind schemes for 2x2 system of balance laws*, Proceedings of the XVI International Conference on Hyperbolic Problems, Springer, (2018), pp. 345–361.

[12] B. Cockburn and C.-W. Shu, *TVB Runge-Kutta local projection discontinuous Galerkin finite element method for conservation laws. II. General framework*, Math. Comp., 52 (1989), pp. 411–435.

[13] ——, *The local discontinuous Galerkin method for time-dependent convection-diffusion systems*, SIAM J. Numer. Anal., 35 (1998), pp. 2440–2463.

[14] R. M. Colombo and M. Garavello, *A well posed Riemann problem for the p-system at a junction*, Netw. Heterog. Media, 1 (2006), pp. 495–511.

[15] R. Courant and K. O. Friedrichs, *Supersonic Flow and Shock Waves*, Interscience Publishers, Inc., New York, N. Y., 1948.

[16] L. Gascón and J. M. Corberán, *Construction of second-order TVD schemes for nonhomogeneous hyperbolic conservation laws*, J. Comput. Phys., 172 (2001), pp. 261–297.

[17] S. K. Godunov, *The problem of a generalized solution in the theory of quasi-linear equations and in gas dynamics*, Uspehi Mat. Nauk, 17 (1962), pp. 147–158.

[18] T. J. R. Hughes, L. P. Franca, and M. Mallet, *A new finite element formulation for computational fluid dynamics. I. Symmetric forms of the compressible Euler and Navier-Stokes equations and the second law of thermodynamics*, Comput. Methods Appl. Mech. Engrg., 54 (1986), pp. 223–234.

[19] R. Käppeli and S. Mishra, *Well-balanced schemes for the Euler equations with gravitation*, J. Comput. Phys., 259 (2014), pp. 199–219.

[20] R. J. LeVeque, *Numerical methods for conservation laws*, Lectures in Mathematics ETH Zürich, Birkhäuser Verlag, Basel, second ed., 1992.

[21] Y. Mantri, H. Herty, and S. Noelle, *Well-balanced scheme for gas-flow in pipeline networks*, Netw. Heterog. Media, 14 (2019), pp. 659–676.

[22] M. S. Mock, *Systems of conservation laws of mixed type*, J. Differential Equations, 37 (1980), pp. 70–88.

[23] A. Morin and G. A. Reigstad, *Pipe networks: Coupling constants in a junction for the isentropic euler equations*, Energy Procedia, 64 (2015), pp. 140–149.

[24] S. Noelle, N. Pankratz, G. Puppo, and J. R. Natvig, *Well-balanced finite volume schemes of arbitrary order of accuracy for shallow water flows*, J. Comput. Phys., 213 (2006), pp. 474–499.

[25] S. Noelle, Y. Xing, and C.-W. Shu, *High-order well-balanced finite volume WENO schemes for shallow water equation with moving water*, J. Comput. Phys., 226 (2007), pp. 29–58.

[26] G. A. Reigstad, *Existence and uniqueness of solutions to the generalized Riemann problem for isentropic flow*, SIAM J. Appl. Math., 75 (2015), pp. 679–702.